Modeling Deformable Shell-like Objects Grasped by a Robot Hand

Jiang Tian and Yan-Bin Jia

Abstract— This paper models (large) deformations of shell-like objects under the grasping of a robot hand. Classical nonlinear theory of thin shells [21, pp. 186-194] is generalized to shells with arbitrary parametric middle surfaces, using a method introduced in our earlier work [13]. An experimental study demonstrates higher modeling accuracy using the nonlinear elasticity theory than its linear counterpart. Given that many deformable objects undergo sizable shape changes when they are grasped, our result supports the application of nonlinear elasticity theory in the future design of grasp strategies for this type of objects.

I. INTRODUCTION

We deal with deformable objects everyday in our life. Examples include clothes, plastic bottles, paper, magazines, ropes, wires, cables, balls, tires, toys, sofas, fruits, vegetables, meat, processed food (e.g., cakes, dumplings, buns, noodles), plants, pets, biological tissues, and so on. The ability to manipulate deformable objects is an indispensable part of the human hand's dexterity and an important feature of intelligence.

In robotics, though much research has been done on planning and manipulation that involve rigid objects, not until recently did deformable objects start to get attention from a critical mass of researchers. Work in this new area has primarily targeted linear [26], [19] and meshed [9] deformable objects. In particular, some researchers [24], [18], [15] have investigated knotting and unknotting with ropes and wires. Meanwhile, only a fraction of existing work has been demonstrated through robot experiments.

In a grasping task, since the number of degrees of freedom of a deformable object is infinite, it cannot be restrained by only a finite set of contacts. Consequently, form closure is no longer applicable. Does force closure still apply? Consider two fingers squeezing a deformable object in order to grasp it. The normal at each contact point changes its direction, so does the corresponding contact friction cone. Even though the initial finger placement may be far from being antipodal, after the deformation the intersection of the contact friction cones could still contain the line segment connecting the two contact points, resulting in a force-closure grasp. To understand the grasping process, deformable modeling plays a very important role.

This paper experimentally investigates shape modeling for shell-like objects that are grasped by a robot hand. A shell is a thin body bounded by two curved surfaces whose distance (i.e., the shell thickness) is very small in comparison with the other dimensions. The locus of points at equal distances

Department of Computer Science, Iowa State University, Ames, IA 50011, USA. `jiangt, jia@cs.iastate.edu`.

from the two bounding surfaces is the *middle surface* of the shell. All shells in this paper are considered *isotropic*, i.e., having the same elastic properties in all directions.

Linear theory of thin shells [20] make simplifications that ignore elongations and shears in comparison to unity, as well as products of angles of rotation in comparison to elongations and shears. The theory may introduce sizable errors in grasping a shell-like object such as a ball, which often results in a large deformation. This was confirmed in our previous work [13].

This paper employs nonlinear theory of elasticity [21], which deals with geometrically nonlinear (i.e., with large angles of rotation) but physically linear (i.e., obeying Hooke's law) problems. The deformation of a grasped object is determined through minimizing its potential energy (which equals its strain energy subtracting the work done by the robot hand to achieve the grasp).

The strain energy of a deformed shell depends on the geometry of its middle surface and thickness, all prior to the deformation, as well as the displacement field. In this paper, we will rewrite strains in terms of geometric invariants, essentially extending our transformation of linear shell theory [13] to the nonlinear case.

We present an experimental study of the modeling of deformations generated by two-finger grasping, where the results yielded by linear and nonlinear theories of shells will be compared.

Section II surveys related work in the FEM for shells and other deformable modeling work in robotics. Section III reviews the theory of nonlinear elasticity of shells, expressing strains in terms of geometric invariants to make the theory directly applicable to arbitrary parametric surfaces. Section IV sets up the subdivision-based displacement field and describes the minimization process. Section V experimentally investigates the modeling of deformable objects grasped by a BarrettHand. It compares the linear theory for small deformations and the nonlinear theory for large deformations through validation against range data generated by a 3D scanner. We will see that nonlinear elasticity based modeling yields much more accurate results. Section VI discusses future improvements on modeling, and links to the next phase of our research on grasping of deformable objects.

II. RELATED WORK

The Finite Element Method (FEM) [8], [25], [2], for modeling the deformations of a wide range of shapes, represents a body as a mesh structure, and computes the stress, strain, and displacement everywhere inside the body. Thin shell finite elements, originated in the mid-1960s, typically include

flat plates [29], axisymmetric shells [10], [22], and curve elements [5]. More recently, computational shell analysis in the FEM has employed techniques including degenerated shell approach [11], stress-resultant-based formulations [1], integration techniques [3], 3-D elasticity elements [6], etc. For more on thin shell finite elements, we refer the reader to two comprehensive surveys [27], [28] which cover work before 1985 and from then on to 2000, respectively.

Due to heavy computation, FEMs often have to be simulated off-line, and do not model large deformations well. FEMs for shells [14], due to their nature of discretization, inaccurately treat higher order geometric invariants such as curvature and torsion. The use of the closed-form energy formulation could alleviate such problem. Nonlinear FEMs (NFEMs) [23] work on large deformations, only at increasing computational cost.

The boundary element method (BEM) [12] solves displacements and forces on the boundary surface, and thus is more efficient than the FEM.

In a contact-based task such as grasping or dexterous manipulation, it is often sufficient to model deformations of the contact regions only. The skeleton-based method [17] computes the stresses/strains only at contact points and geometrically salient points and then interpolates over the entire surface.

In our previous work [13], the strain-displacement and strain energy equations from classical (linear) theory of shells [20] were transformed to become applicable to shells with arbitrary parametric middle surfaces. This paper applies *nonlinear* elasticity theory to model large deformations of shell-like objects that are grasped by a robot hand.

To see the difference between nonlinear and linear elasticity theories, we look at the simple example of a rotation about the z-axis through an angle θ, which results in the position change:

$$
\left(\begin{array}{c} u \\ v \\ w \end{array} \right) = \left(\begin{array}{ccc} \cos\theta & -\sin\theta & 0 \\ \sin\theta & \cos\theta & 0 \\ 0 & 0 & 1 \end{array} \right) \left(\begin{array}{c} x \\ y \\ z \end{array} \right) - \left(\begin{array}{c} x \\ y \\ z \end{array} \right).
$$

No deformation is involved, hence no strain, as confirmed by the nonlinear theory:

$$
\begin{aligned}
\epsilon_x &= \frac{\partial u}{\partial x} + \frac{1}{2}\left[\left(\frac{\partial u}{\partial x}\right)^2 + \left(\frac{\partial v}{\partial x}\right)^2 + \left(\frac{\partial w}{\partial x}\right)^2 \right] \\
&= \cos\theta - 1 + \frac{1}{2}\left[(\cos\theta - 1)^2 + (\sin\theta)^2 \right] \\
&= 0.
\end{aligned}
$$

However, linear elasticity theory yields a strain

$$
\epsilon_x = \frac{\partial u}{\partial x} = \cos\theta - 1.
$$

III. Nonlinear Elasticity of Shells

Let $\boldsymbol{\sigma}(u, v)$ be the middle surface of an isotropic thin shell, as shown on the left in Fig. 1. It is regular in that the tangent plane at every point is spanned by the two partial derivatives $\boldsymbol{\sigma}_u$ and $\boldsymbol{\sigma}_v$. At a point $\boldsymbol{q} = \boldsymbol{\sigma}(u, v)$ in the middle surface the Darboux frame consists of the unit surface normal $\boldsymbol{n}$ and the
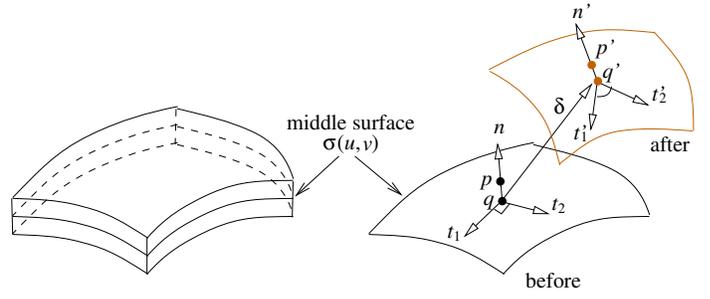
Fig. 1. Deformation of a shell. The point $\boldsymbol{p}$ in the shell is along the direction of the normal $\boldsymbol{n}$ at the point $\boldsymbol{q}$ on the middle surface.

two unit principal vectors $\boldsymbol{t}_1$ and $\boldsymbol{t}_2$. Under a deformation, the displacement of $\boldsymbol{q}$ is given as

$$
\boldsymbol{\delta}(u, v) = \alpha(u, v)\boldsymbol{t}_1 + \beta(u, v)\boldsymbol{t}_2 + \gamma(u, v)\boldsymbol{n}.
$$

Kirchhoff's assumption states that *straight fibers normal to the middle surface of a shell before the deformation remain straight and normal to the middle surface after the deformation.* Under the assumption, the relative elongation ε_{33} of a fiber along the normal $\boldsymbol{n}$, and shears ε_{13} and ε_{23}, respectively, in the $\boldsymbol{t}_1$-$\boldsymbol{n}$ and $\boldsymbol{t}_2$-$\boldsymbol{n}$ planes (before the deformation), are zero; namely,

$$
\varepsilon_{33} = \varepsilon_{13} = \varepsilon_{23} = 0. \tag{1}
$$

Consider a point $\boldsymbol{p} = \boldsymbol{q} + z\boldsymbol{n}$ in the shell; so, $\boldsymbol{q}$ is the projection of $\boldsymbol{p}$ on the middle surface and z the (signed) distance. The displacement of $\boldsymbol{p}$ assumes the form

$$
\boldsymbol{\delta}(u, v) + z \left(\begin{array}{c} \vartheta(u, v) \\ \varphi(u, v) \\ \chi(u, v)) \end{array} \right). \tag{2}
$$

Classical theory of shells assumes the middle surface of a shell to be a principal patch, that is, its partial derivatives to be along the principal directions at every point. We here use the treatment of large deformations of shells in [21, pp. 186-194]. To make the theory applicable to an arbitrary parametric middle surface, we apply the technique in [13] to rewrite strains and shears in terms of geometric invariants. These invariants include principal curvatures, their derivatives with respect to the principal vectors, and the covariant derivatives of the principal vectors with respect to each other.

Let f and $\boldsymbol{t}$ be a function and a tangent vector field defined on the surface $\boldsymbol{\sigma}$, respectively. Denote by $\boldsymbol{t}[f]$ the directional derivative of f with respect to $\boldsymbol{t}$, and by $\nabla_t\boldsymbol{w}$ the covariant derivative of another vector field $\boldsymbol{w}$ with respect to $\boldsymbol{t}$. At the point $\boldsymbol{q}$ on the middle surface, we have

$$
\begin{aligned}
\boldsymbol{t}[f] &= \lim_{\Delta s \to 0} \frac{f(\boldsymbol{q} + \Delta s \cdot \boldsymbol{t}) - f(\boldsymbol{q})}{\Delta s}, \\
\nabla_t\boldsymbol{w} &= \lim_{\Delta s \to 0} \frac{\boldsymbol{w}(\boldsymbol{q} + \Delta s \cdot \boldsymbol{t}) - \boldsymbol{w}(\boldsymbol{q})}{\Delta s}.
\end{aligned}
$$

At $\boldsymbol{q}$, let ϵ_i, $i = 1, 2$, be the relative elongation of an infinitesimal segment (which was in the principal direction

t_i before the deformation) as projected onto t_i:

$$\epsilon_1 = t_1[\alpha] + (\nabla_{t_1} t_2 \cdot t_1)\beta + (\nabla_{t_1} n \cdot t_1)\gamma, \quad (3)$$
$$\epsilon_2 = t_2[\beta] + (\nabla_{t_2} t_1 \cdot t_2)\alpha + (\nabla_{t_2} n \cdot t_2)\gamma, \quad (4)$$

For example, ϵ_1 consists of the change rate of the displacement α along t_1, and two components in the same direction indirectly caused by the displacements in the two orthogonal directions t_2 and n.

Under the deformation, the rotations of the principal vectors t_1 and t_2 about the normal n toward each other, respectively, are:

$$\omega_1 = t_2[\alpha] - (\nabla_{t_2} t_1 \cdot t_2)\beta, \quad (5)$$
$$\omega_2 = t_1[\beta] - (\nabla_{t_1} t_2 \cdot t_1)\alpha, \quad (6)$$

In (5), for example, the first term represents the rotation of t_1 toward t_2 due to the change in the displacement α (defined in t_1) along t_2. The second term, to be subtracted from the first, is the rotation amount that ought to happen due to the variation of t_1 along t_2 and the displacement β in the latter tangent direction.

Similarly, the next two terms quantify the rotations of the surface normal n about t_2 (t_1, respectively) toward t_1 (t_2, respectively):

$$\phi_1 = -t_1[\gamma] + (\nabla_{t_1} n \cdot t_1)\alpha, \quad (7)$$
$$\phi_2 = -t_2[\gamma] + (\nabla_{t_2} n \cdot t_2)\beta. \quad (8)$$

By definition, $-\nabla_{t_1} n \cdot t_1$ and $-\nabla_{t_2} n \cdot t_2$ are the *principal curvatures* in t_1 and t_2, respectively.

For a large deformation, we obtain the relative elongations of infinitesimal line elements starting at q which, before the deformation, were parallel to the two principal directions t_1 and t_2, respectively:

$$\hat{\varepsilon}_{11} = \epsilon_1 + \frac{1}{2}(\epsilon_1^2 + \omega_1^2 + \phi_1^2), \quad (9)$$
$$\hat{\varepsilon}_{22} = \epsilon_2 + \frac{1}{2}(\epsilon_2^2 + \omega_2^2 + \phi_2^2), \quad (10)$$

as well as the shear in the tangent plane:

$$\hat{\varepsilon}_{12} = \omega_1 + \omega_2 + \epsilon_1\omega_2 + \epsilon_2\omega_1 + \phi_1\phi_2. \quad (11)$$

Note the appearance of nonlinear terms in equations (9)–(11).

The rate of displacement in (2) along the normal n at q is determined from the six strain components (3)–(8):

$$\vartheta = \phi_1(1 + \epsilon_2) - \phi_2\omega_1, \quad (12)$$
$$\varphi = \phi_2(1 + \epsilon_1) - \phi_1\omega_2, \quad (13)$$
$$\chi = \epsilon_1 + \epsilon_2 + \epsilon_1\epsilon_2 - \omega_1\omega_2. \quad (14)$$

The relative elongations and shear at p off the middle surface are affected by the second order changes in geometry at its projection q in the middle surface. They are characterized

by the following "curvature" terms:

$$\kappa_{11} = t_1[\vartheta] + (\nabla_{t_1} t_2 \cdot t_1)\varphi + (\nabla_{t_1} n \cdot t_1)\chi,$$
$$\kappa_{22} = t_2[\varphi] + (\nabla_{t_2} t_1 \cdot t_2)\vartheta + (\nabla_{t_2} n \cdot t_2)\chi,$$
$$\kappa_{12} = t_1[\varphi] - (\nabla_{t_1} t_2 \cdot t_1)\vartheta,$$
$$\kappa_{21} = t_2[\vartheta] - (\nabla_{t_2} t_1 \cdot t_2)\varphi,$$
$$\kappa_{13} = t_1[\chi] - (\nabla_{t_1} n \cdot t_1)\vartheta,$$
$$\kappa_{23} = t_2[\chi] - (\nabla_{t_2} n \cdot t_2)\varphi.$$

Among them, κ_{11} and κ_{22} describe the changes in curvature along t_1 and t_2; κ_{12} and κ_{21} together describe the twist of the middle surface in the tangent plane; and κ_{13} and κ_{23} describe the twists out of the tangent plane.

The six terms κ_{ij} form the following three parameters that together characterize the variations of the curvatures of the middle surface:

$$\zeta_{11} = (1 + \epsilon_1)\kappa_{11} + \omega_1\kappa_{12} - \phi_1\kappa_{13}, \quad (15)$$
$$\zeta_{22} = (1 + \epsilon_2)\kappa_{22} + \omega_2\kappa_{21} - \phi_2\kappa_{23}, \quad (16)$$
$$\zeta_{12} = (1 + \epsilon_1)\kappa_{21} + (1 + \epsilon_2)\kappa_{12}$$
$$+ \omega_2\kappa_{11} + \omega_1\kappa_{22} - \phi_2\kappa_{13} - \phi_1\kappa_{23}. \quad (17)$$

Finally, we have the relative tangential elongations and shear at p in terms of those at q in the middle surface:

$$\varepsilon_{11} = \hat{\varepsilon}_{11} + z\zeta_{11}, \quad (18)$$
$$\varepsilon_{22} = \hat{\varepsilon}_{22} + z\zeta_{22}, \quad (19)$$
$$\varepsilon_{12} = \hat{\varepsilon}_{12} + z\zeta_{12}. \quad (20)$$

We have neglected terms in z^2, as well as products of z with the principal curvatures $-\nabla_{t_2} n \cdot t_2$ and $-\nabla_{t_2} n \cdot t_2$.

For small deformations, we neglect elongations and shears compared to unity, for instance, $1 + \epsilon_1 \approx 1$ in (15), as well as their products (also with curvature terms) such as $\epsilon_1\omega_2$ in (11). Equations (18)–(20) then reduce to

$$\varepsilon_{11} = \epsilon_1 + z\kappa_{11},$$
$$\varepsilon_{22} = \epsilon_2 + z\kappa_{22},$$
$$\varepsilon_{12} = \omega_1 + \omega_2 + z(\kappa_{12} + \kappa_{21}),$$

which is the linear elasticity theory of shells.

The strain energy of the shell is an integral over the middle surface S:

$$U_\varepsilon = \frac{e}{2(1 - \mu^2)} \int_S \left\{ h\left(\hat{\varepsilon}_{11}^2 + \hat{\varepsilon}_{22}^2 + 2\mu\hat{\varepsilon}_{11}\hat{\varepsilon}_{22} + \frac{1 - \mu}{2}\hat{\varepsilon}_{12}^2 \right) \right.$$
$$\left. + \frac{h^3}{12}\left(\zeta_{11}^2 + \zeta_{22}^2 + 2\mu\zeta_{11}\zeta_{22} + \frac{1 - \mu}{2}\zeta_{12}^2 \right) \right\}$$
$$\sqrt{EG - F^2}\, du dv. \quad (21)$$

Here $\sqrt{EG - F^2}\, du dv$ is the area element for the integral.

IV. SUBDIVISION-BASED ENERGY MINIMIZATION

Recently, shape functions used for subdivision surfaces have been utilized as finite element basis functions for the simulation of the deformation of thin shells [4]. In equation (21), ζ_{11}, ζ_{22}, and ζ_{12} characterize the variations of the curvatures of the middle surface. They contain second order

derivatives of the displacement. In order to ensure that the bending energy is finite, the basis function interpolating the displacement field and its first- and second-order derivatives have to be square integrable. Loop's subdivision scheme meets such requirement [16].

In a subdivision-based finite element, the basis functions supporting an element are those which correspond to nodes in the neighborhood of the current face of the control mesh. The displacement field within the shaded element in Fig. 2
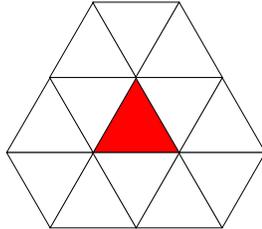

Fig. 2.   A regular patch with 12 control points.

depends on the displacements of the nodes defining the element and of all the immediately adjacent nodes in the triangulation.

$$\boldsymbol{\delta}(u, v) = \sum_{i=1}^{12} N_i(u, v)\boldsymbol{\delta}_i \qquad (22)$$

where $\boldsymbol{\delta}_i$ is the displacement of the ith control point in the neighborhood domain, and $N_i(u, v)$ is the basis function.

Since at the equilibrium state the shell has minimum total potential energy [7, p. 260], we can obtain the displacement field as follows. Differentiate the total potential energy with respect to the displacement coordinates of the control points of the subdivision. Setting the partial derivatives to zero, we have a system of equations.

Small deformations are governed by linear elasticity theory, the resulting linear equations can be easily solved. In comparison, large deformations are governed by a system of nonlinear equations that often has to be solved iteratively. An initial displacement field is generated as follows. The displacement of a point in the neighborhood of some contact point is approximated by a linear function in the distance between these two points and proportional to the force exerted at the contact point. Minimization is conducted toward the radius of the deformed area. After that, the conjugate gradient method is used to refine the results. Each minimization step is performed along the conjugate direction of several preceding gradients. The iteration continues until the gradient becomes zero when a local minimum of the total potential energy is reached. Interpolation in the local neighborhood improves the computational efficiency for nonlinear method. It usually takes several minutes to compute the deformation compared with several seconds for linear case.

V. EXPERIMENT

As shown in Fig. 3, the experimental setup includes an Adept Cobra 600 manipulator, a three-fingered BarrettHand, and a NextEngine's desktop 3D scanner. Every finger of
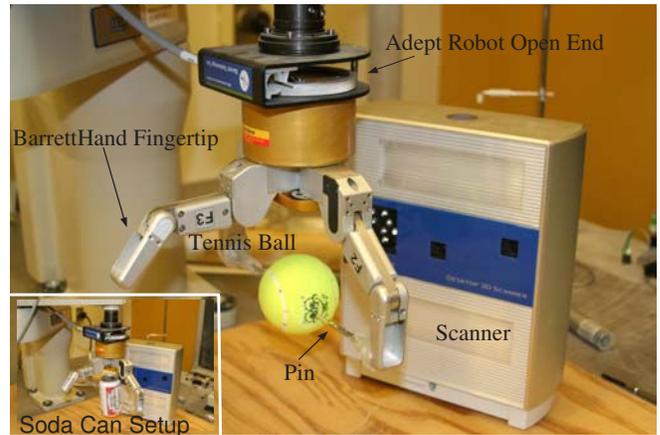

Fig. 3.   Experimental setup with a tennis ball and a soda can (lower left).

the BarrettHand has a strain gauge sensor that measures contact force. To model point contact, a pin is mounted on each of the two grasping fingers. A triangular mesh model of the deformed surface due to finger contact is generated by the NextEngine's desktop 3D scanner with an accuracy of 0.127mm. In our experiment, we measure the modeling accuracy by matching the computed deformed surface against the corresponding mesh model and averaging the distances from the mesh vertices to the deformed surface.

In our previous work [13], we used the linear elasticity theory to model deformation of half of a soda can. By incorporating nonlinear elasticity theory, the average modeling error has decreased from 0.36mm to 0.21mm (see the setup at the left bottom corner of Fig. 3). The last row in Table I displays the scanned image of the deformed can and those constructed using the nonlinear and linear methods.

For further comparison, we have also conducted experiment on a tennis ball grasped at antipodal positions by BarrettHand (show in Fig. 3). The ball has a diameter of 65.0mm. Its rubber has thickness of 2.5mm. We choose the rubber's Young's modulus of 1MPa, and Poisson's ratio of 0.5. Point contact is assumed between the ball and the finger. We use two subdivision-based displacement fields, one for each finger contact. Each subdivision patch is defined over a $45\text{mm} \times 45\text{mm}$ patch, which is large enough to describe the deformed area based on our observation.

Table I displays the comparison results. The first column in the table lists the exerted forces on each finger. The second and third columns list the deformed shapes produced by the scanner. The next two pairs of columuns present the corresponding deformations computed according to the nonlinear and linear elasticity theories, respectively. In the table, each row corresponds to one instance of deformation. The first four shapes result from grasping the tennis ball.

From the table, the nonlinear modeling results have smaller errors than the linear modeling results in four out of five rows, all corresponding to large deformations. For the small deformation in the first row, the two simulation results have comparable errors, which suggests the deformation

force (lbf)	scanned deformation		nonlinear deformation		linear deformation	
	shape	measured max disp. (mm)	shape	average error (mm)	shape	average error (mm)
2.39		2.56		0.31		0.30
3.71		6.05		0.62		0.85
4.58		9.12		0.81		2.0
4.83		10.27		0.65		2.37
0.17		1.42		0.21		0.36
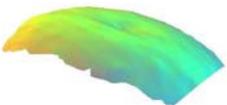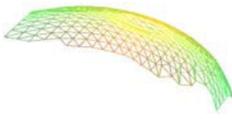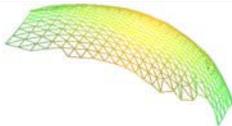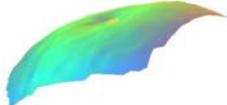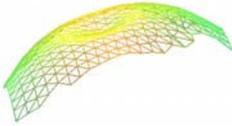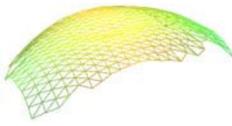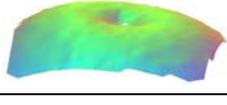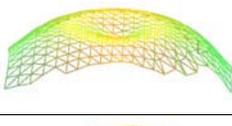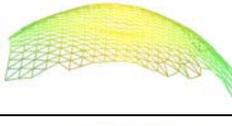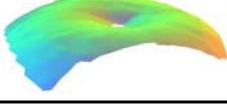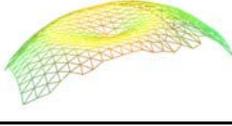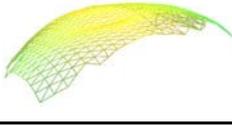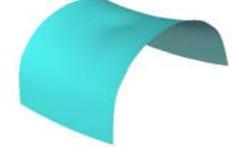
TABLE I

COMPARISONS BETWEEN LINEAR AND NONLINEAR DEFORMATIONS ON A TENNIS BALL (FIRST TO FOURTH ROW) AND A SODA CAN (LAST ROW).

is within the range of linear elasticity. Starting from the second row, the two methods generate shapes that are visibly different from each other. In the second instance, the shape generated by the nonlinear method has an obvious dent comparable to the one on the real shape shown to the left, whereas the shape by the linear method to the right hardly shows any dent. We see that the larger the force, the bigger the difference between nonlinear and linear deformations. The results suggest that the nonlinear method yields small modeling errors when large deformations occur.

Grasping causes deformations in the regions around the contact while the rest of the surface hardly deforms. Fig. 4 shows the deformed regions, under the finger force of 4.83lbf, superposed onto the scanned undeformed model of the tennis ball. The red curves, one at the top and the other at the bottom, mark the borders of these deformed regions. The measured maximum displacement of 10.27mm is achieved at the dark points. Due to symmetry, we only display the top deformed area. We see that the two antipodal contact points move closer under the force exerted by the two fingers. The scanned deformations on the tennis ball and the nonlinear results are within 7% of each other from the fourth row of Table I.

Several factors have affected the accuracy of modeling: occlusions to the scanner, accuracy of the scanner, errors in

Max deformation point
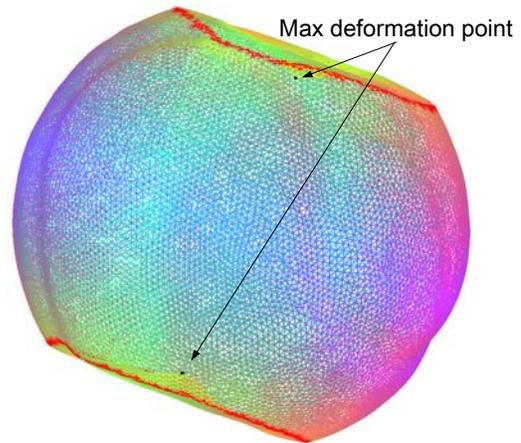
Fig. 4. Deformed tennis ball under grasping. The points in contact with the fingers have maximum displacments of 10.27mm.

the force readings, and the air pressure inside the tennis ball. Because the scanner is much larger than the tennis ball and the BarrettHand fingers, the deformed shape is scanned at different orientations and the resulting patches are combined. This process introduces errors. During the experiments, the zero point of the BarrettHand's strain gauge sensors tends to drift a little bit, leading to errors in force readings. Finally,

the air inside the ball also influences the deformation, and this effect is not modeled in the experiment.

VI. Discussion

The experimental results indicate the existence of a state of deformation at which the modeling should switch from linear elastic to nonlinear elastic. Though the nonlinear elasticity theory of shells suggest simplifications that would turn the problem into a linear one for small deformations, a further empirical investigation is needed given the inaccuracy of (even) the nonlinear model due to its assumptions, measurement errors of the physical constants, and other uncertainties. In real time modeling of, say, grasping, computational time can be critical. A linear elastic model is more efficient than a nonlinear elastic model, it would be very useful to gauge the transition point.

Employing the closed form of strain energy in replacement of discretization-based differentiation, our method follows the physics of elasticity more closely and is expected to be more accurate than the FEM. We will compare the modeling performances of the FEM and our method in the near future.

The presented work assumes point finger contacts. In practice, as the robot fingers press a deformable object to secure a grasp, the contact regions grow larger. Under such a circumstance, modeling should be improved by considering area contacts and distributed loads. Tactile array sensors will be installed on the BarrettHand for dynamic detection of contact regions on the fingertips. It would also be interesting to examine the relationship between an object's energy and its equilibrium grasp.

An antipodal grasp typically results in deformations in small parts of an object. One objective in the future is to simulate twisting and bending of a grasped object. In this case, it is even more important to use the nonlinear model since linear deformations do not model rotations well, and can yield distortions when displacements are global.

In the future, we would also like to consider solid objects which are more common in a robot task than shell-like objects. One plan is to develop an interactive environment that can model deformations of shell-like and solid objects as the shape changes. Such an interface will facilitate the analysis or synthesis of grasp strategies for these types of objects.

VII. Acknowledgment

References

[1] J. H. Argyris and D. W. Scharpf. The SHEBA family of shell elements for the matrix displacement method. Part I. Natural definition of geometry and strains. *Journal of the Royal Aeronautical Society*, 72:873–878, 1968.

[2] K. J. Bathe. *Finite Element Procedures*. Prentice Hall, 1996.

[3] T. Belytschko and C. Tsay. A stabilization procedure for the quadrilateral plate element with one-point quadrature. *International Journal of Numerical Methods in Engineering*, 19:405–419, 1983.

[4] F. Cirak, M. Ortiz, and P. Schröder. Subdivision surfaces: a new paradigm for thin-shell finite-element analysis. *International Journal for Numerical Methods in Engineering*, 47(12):2039–2072, 2000.

[5] J. J. Connor and C. A. Brebbia. A stiffness matrix for a shallow rectangular shell element. *Journal of Engineering Mechanics Division*, 93(5):43–65, 1967.

[6] A. Dorfmann and R. B. Nelson. Three-dimensional finite element for analyzing thin plate/shell structures. *International Journal of Numerical Methods in Engineering*, 38:3453–3482, 1995.

[7] R. T. Fenner. *Engineering Elasticity: Application of Numerical and Analytical Techniques*. Ellis Horwood, Ltd., 1986.

[8] R. H. Gallagher. *Finite Element Analysis*. Prentice-Hall, Inc., 1975.

[9] K. Gopalakrishnan and K. Goldberg. D-space and deform closure grasps of deformable parts. *International Journal of Robotics Research*, 24(11):899–910, 2005.

[10] P. E. Grafton and D. R. Strome. Analysis of axisymmetric shells by the direct stiffness method. *AIAA journal*, 3:2138–2145, 1963.

[11] T. J. R. Hughes and W. K. Liu. Nonlinear finite element analysis of shells: Part I. Three-dimensional shells. *Computational Methods in Applied Mechanics and Engineering*, 26:331–362, 1981.

[12] D. L. James and D. K. Pai. Artdefo: accurate real time deformable objects. In *Proceedings of ACM SIGGRAPH*, pages 65–72, 1999.

[13] Y.-B. Jia and J. Tian. Deformations of general parametric shells: computation and experiment. In *Proceedings of the IEEE/RSJ International Conference on Intelligent Robots and Systems*, pages 1796–1803, 2008.

[14] C. S. Krishnamoorthy. *Finite Element Analysis: Theory and Programming*. Tata McGraw-Hill Publishing, Ltd., New Delhi, 2nd edition, 1995.

[15] A. M. Ladd and L. E. Kavraki. Using motion planning for knot untangling. *International Journal of Robotics Research*, 23(7):797–808, 2004.

[16] C. Loop. *Smooth subdivision surfaces based on triangles*. Master's thesis, University of Utah, 1987.

[17] Q. Luo and J. Xiao. Contact and deformation modeling for interactive environments. *IEEE Transactions on Robotics*, 23(2):416–430, 2007.

[18] T. Matsuno and T. Fukuda. Manipulation of flexible rope using topological model based on sensor information. In *Proceedings of the IEEE/RSJ International Conference on Intelligent Robots and Systems*, pages 2638–2643, 2006.

[19] M. Moll and L. E. Kavraki. Path planning for deformable linear objects. *IEEE Transactions on Robotics and Automation*, 22(4):625–636, 2006.

[20] V. V. Novozhilov. *The Theory of Thin Shells*. P. Noordhoff Ltd., 1959.

[21] V. V. Novozhilov. *Foundations of the Nonlinear Theory of Elasticity*. Dover Publications, Inc., 1999.

[22] E. P. Popov, J. Penzien, and Z. A. Lu. Finite element solution for axisymmetric shells. *Journal of Engineering Mechanics Division, ASCE*, 90(5):119–145, 1965.

[23] J. N. Reddy. *An Introduction to Nonlinear Finite Element Analysis*. Oxford University Press, 2004.

[24] M. Saha and P. Isto. Motion planning for robotic manipulation of deformable linear objects. In *Proceedings of the IEEE International Conference on Robotics and Automation*, pages 2478–2484, 2006.

[25] L. Segerlind. *Applied Finite Element Analysis*. John Wiley and Sons, New York, 1984.

[26] H. Wakamatsu and S. Hirai. Static modeling of linear object deformation based on differential geometry. *International Journal of Robotics Research*, 23(3):293–311, 2004.

[27] H. T. Y. Yang, S. Saigal, and D. G. Liaw. Advances of thin shell finite elements and some applications — version 1. *Computers and Structures*, 35(4):481–504, 1990.

[28] H. T. Y. Yang, S. Saigal, A. Masud, and R. K. Kapania. A survey of recent shell finite elements. *International Journal for Numerical Methods in Engineering*, 47:101–127, 2000.

[29] O. C. Zienkiewicz. *The Finite Element Method*. McGraw-Hill, 3rd edition, 1979.